Flow Measurement and Instrumentation 66 (2019) 99–110

Contents lists available at ScienceDirect

Flow Measurement and Instrumentation

journal homepage: www.elsevier.com/locate/flowmeasinst

Mean velocity and turbulent characteristics of flow over half-cycle cosine sharp-crested weirs

Saeed Salehi[a], Kazem Esmaili[a], Amir H. Azimi[b,*]

[a] Dept. of Agriculture Engineering, Ferdowsi University of Mashhad, Mashhad, Iran
[b] Dept. of Civil Engineering, Lakehead University, Thunder Bay, ON, P7B 5E1, Canada

ARTICLE INFO

Keywords:
Flow discharge
Flow measurement
Hydraulics
Cosine weir
Sharp-crested weir
Submerged flow
Turbulence
Turbulent kinetic energy

ABSTRACT

The classical sharp-crested weirs are not suitable to implement in irrigation canals with high suspended sediment flow. Over the time, sediment deposition occurs in the upstream of sharp-crested weirs and causes a time variant water level raise in the upstream and consequently variable discharge coefficients. A series of laboratory experiments was carried out to test the hypothesis of strong turbulent formation and three-dimensional flow in the upstream of half-cosine sharp-crested weirs to prevent sediment deposition. To verify this hypothesis, a series of laboratory experiment was carried out for different weir heights and top widths in free and submerged flow conditions. Mean flow structure and turbulent characteristics of half-cosine and rectangular sharp-crested weirs were measured using a micro-Acoustic Doppler Velocimeter (ADV) probe. It was found that the streamwise velocities of half-cosine weirs were higher than the corresponding rectangular weirs, however, the velocity fluctuations in this direction were similar for both types of weirs. Velocity fluctuations in vertical and transverse directions were found to be significant in half-cosine weirs. The results showed higher turbulent kinetic energy below the crest level for half-cosine weirs which made them capable of sediment resuspension and sediment removal. In was found that the introduced weir model are suitable structures for passage of small floating debris and sediments. A head-discharge formulation was also developed based on the geometry of half-cosine weir in free flow and a constant discharge coefficient was obtained by solving the Fresnel integrals. For practical purposes, semi-empirical formulations were also developed to estimate flow discharge in both free and submerged flow conditions.

1. Introduction

Weirs are commonly used in civil engineering for flow measurement and as flow controlling structures to control the upstream water level. In addition, weirs can be employed to increase water storage, enhance irrigation capacity, and enable navigation in shallow channels [1]. Using Bernoulli's principle provides a unique correlation between the upstream water head h_o and the flow discharge Q_f. This relationship enables weirs to be used as a flow measuring structure. The weirs in general can be classified into sharp-crested weirs and weirs of finite crest length [1–3]. Sharp-crested weirs have smaller flow capacity in comparison with weirs of finite crest length and they are usually being used in laboratories and in small channels. Sharp-crested weirs can be designed in many different shapes such as rectangular, triangular, trapezoidal, and half-circular [1,4–12]. Many laboratory experiments and numerical simulations have been performed to develop and generalize formulations for prediction of the head-discharge relationships for sharp-crested weirs, inclined weirs, and weirs of finite crest length [13–18].

Baddour [8] developed a method to determine head-discharge equations for sharp-crested weirs with polynomial sections of any order. He presented examples of fourth-order polynomial weirs and stated that such weirs behave similarly to the proportional weirs. Vatankhah [12] implemented the theoretical approach to develop a head-discharge relationship for sharp-crested circular weirs in free flow condition. The proposed equation was compared with experimental data and it showed very small prediction error in the range of 0.1%. Bijankhan and Ferro [10] carried out laboratory experiments on the performance of circular overflow structures and proposed stage-discharge relationships. Recently, Oreizi et al. [19] investigated hydraulic characteristics of flow over one-cycle sinusoidal sharp-crested weirs in free flow condition and a head-discharge equation for prediction of flow rate was proposed. The head-discharge formula was determined by solving the Fresnel sine and cosine integrals and a discharge coefficient.

* Corresponding author.
E-mail addresses: saeedsalehi100@gmail.com (S. Salehi), azimi@lakeheadu.ca (A.H. Azimi).

https://doi.org/10.1016/j.flowmeasinst.2019.02.002
Received 14 November 2017; Received in revised form 22 January 2019; Accepted 16 February 2019
Available online 26 February 2019
0955-5986/

It was reported that the variations of secondary currents in sinusoidal weirs were more considerable than that of rectangular weirs and sinusoidal weirs are suitable for passing sediments and debris due to formation of secondary current and high turbulence. The hydraulic behavior of sinusoidal weirs was also compared with that of rectangular sharp-crested weirs and found that the turbulence intensity in the vicinity of the sinusoidal weirs are stronger than those of rectangular weirs.

Flow over sharp-crested weirs becomes submerged once the downstream water level t (i.e., tailwater) rises above the crest elevation [20]. In this flow condition, the upstream water level will be affected by the downstream water level and the capacity of weirs to pass water decreases significantly. For a sharp-crested weir, the submergence occurs even before the tailwater reaches the crest elevation [21] whereas for weirs of finite crest length and embankment weirs the upstream water level remains unchanged even if the tailwater rises above the crest elevation [22–25].

The aim of the present research study is to introduce a new weir geometry with a half-cycle cosine cross section with different weir heights P, top widths w, and a wide range of discharges. The performance of half-cosine weirs is studied for both free and submerged flow conditions. The overall flow structure including, three-dimensional velocity distributions, and turbulent flow characteristics for both free and submerged flow conditions are studied. In addition, the head-discharge correlation for half-cosine weirs is theoretically developed and the discharge coefficient is calibrated with experimental data.

2. Background

2.1. Discharge coefficient

For free flow over rectangular sharp-crested weirs, the free flow discharge Q_f can be formulated from energy consideration as

$$Q_f = \frac{2}{3} b C_D \sqrt{2g}\, h_o^{3/2} \tag{1}$$

where b is the weir length (equal to the channel width B in which it is located across its full width), g is the gravity acceleration, h_o is the water depth measured from a horizontal reference level localized at an elevation equal to the weir height P and measured $3h_o$-$4h_o$ upstream of the weir [1] and C_D is the discharge coefficient. Since the geometry of the weirs influence the approach velocity in the upstream and over the weirs, discharge coefficients are introduced to reflect these effects. The prediction formulas for discharge coefficient of full-width sharp-crested weirs and rectangular sharp-crested weirs can be found in the literature [1,13,14,16,18,26].

Oreizi et al. [19] investigated the hydraulic characteristics of flow over sinusoidal sharp-crested weirs. A discharge equation was formulated for this type of weirs described by

$$Q_f = \frac{2\sqrt{2g}}{3} C_D \left(b h_o^{3/2} + b_a \frac{3D}{2\pi n} h_o^{1/2} \right) \tag{2}$$

where b_a is the amplitude of the sine function, n is the cycle number, and D is the distance from the weir crest to the highest or lowest point of the sine/cosine waves (see Fig. 1a). A discharge coefficient formula was developed from laboratory data and it can be described by

$$C_D = 0.4 \sin\left(0.77\pi \frac{h_o}{D}\right) + 0.24 \tag{3}$$

2.2. Discharge reduction factor

Vennard and Weston [27] presented a summary of experimental studies pointing out that the discharge reduction factor ψ defined by

$$Q_s = \psi\, Q_f \tag{4}$$

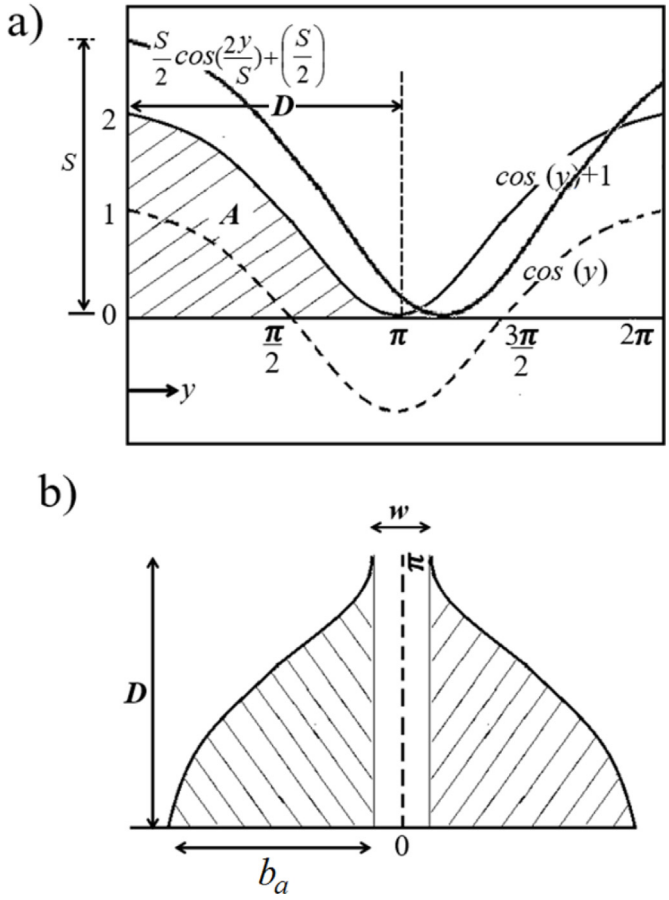

Fig. 1. Definition sketch of a cosine sharp-crested weir; a) cosine profile; b) cosine sharp-crested weir.

where Q_s is the submerged discharge and Q_f is the corresponding free discharge for submerged upstream head h. The discharge reduction factor ψ was found to be a function of both t/h and h_o where t is the tailwater depth [27]. Villemonte [28] developed an empirical equation for sharp-crested weirs to predict the discharge reduction factor as

$$\psi = \left(1 - \frac{t}{h}\right)^{0.385} \tag{5}$$

For deeply submerged sharp-crested weirs (i.e., $t/h > 0.9$), Rajaratnam and Muralidhar [29] proposed an equation to directly predict the discharge in submerged flow condition as

$$Q_s = 0.9\, Bt\sqrt{g(h - t)} \tag{6}$$

Eq. (6) can be rewritten in form of discharge reduction factor as

$$\psi = \frac{0.955}{C_d} \frac{t}{h} \sqrt{1 - \frac{t}{h}} \tag{7}$$

Abou-Seida and Quarishi [6] simplified the submerged flow over a sharp-crested weir as a combination of a free flow with a head $(h-t)$ and an orifice flow with a thickness of t proposing the reduction factor as

$$\psi = \left(1 - \frac{t}{h}\right)^{1/2} \left(1 + \frac{t}{2h}\right) \tag{8}$$

Eq. (8) provides accurate results for $0 < t/h < 0.9$. Wu and Rajaratnam [21] proposed a formula to correlate the discharge reduction factor ψ only as a function of submergence level as

$$\psi = f(t/h) = 1.0 + 1.162(t/h) - 1.331 \sin^{-1}(t/h) \tag{9}$$

The proposed formula can be used for t/h up to about 0.95.

Bijankhan and kouchakzadeh [30] proposed an equation for ψ for submerged triangular labyrinth weir as

$$\psi = \left[1 - \left(\frac{t}{h}\right)^{3/2}\right]^{0.133} \quad (10)$$

3. Experimental setup

Experiments were conducted in a horizontal, rectangular glass-walled flume 10 m long, 0.4 m wide, and 0.6 m high in the Hydraulic Laboratory of the Department of Civil Engineering at the Ferdowsi University of Mashhad, Iran. The weir model was installed 4 m from the flume entrance and screens at the flume entrance reduced the initial surface water fluctuations. The centerline water surface levels on the upstream and downstream of the weir were measured 0.5 m from the weir with mechanical point gauges with an accuracy of ± 0.1 mm. The flow rate over the weir was measured with an inline magnetic flow meter to ± 0.01 L/s accuracy and flow measurements were checked by volumetric flow rate measurements. The discharge fluctuations for low and high discharges varied from ± 0.3% to ± 1% of its average. The downstream water level was controlled by a flap gate located at the flume end to form the modular limit and submerged flow conditions.

In total nine half-cycle cosine sharp-crested weir models with three weir heights of P = 0.13 m, 0.18 m, 0.23 m and three crest widths of b = 0.18 m, 0.21 m, and 0.24 m corresponding to the weir top widths of w = 0 m, 0.03 m, and 0.06 m were made from galvanized steel plates (see Fig. 2) to model the effect of the weir top width w and approach velocity h_o/P on the performance of half-cosine sharp-crested weirs. In addition, three weir models of rectangular sharp-crested weirs with the same weir heights of P = 0.13 m, 0.18 m, 0.23 m were fabricated and tested to be used as the benchmarks for comparison. For each weir model, experiments were conducted with discharges ranging from 3.82 to 21.84 L/s (see Table 1). Laboratory experiments indicated that the flow nappe downstream of the contracted half-cosine weirs was self-aerated and no additional ventilation was required to form aerated nappe (see Fig. 3).

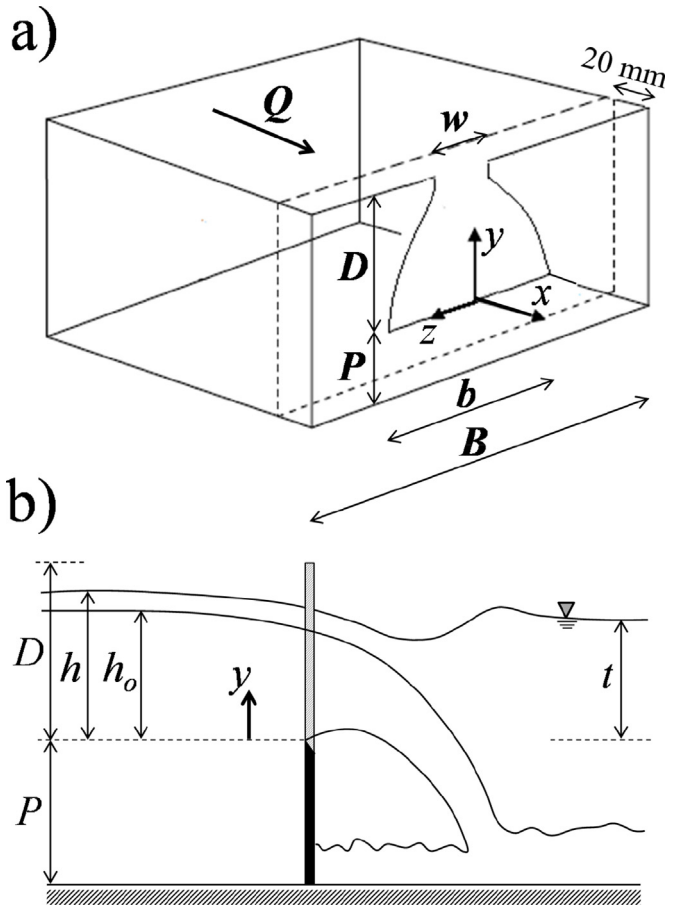

Fig. 2. Three-dimensional sketch of a cosine sharp-crested weir with a Cartesian coordinate system; b) schematic of water surface profile in free and submerged flow conditions.

In order to understand the hydraulics of flow over weirs, important non-dimensional parameters such as Froude $F = Q_f/[gb^2(h_o + P)^3]^{1/2}$, Reynolds number $R = (gh_o^3)^{1/2}/\nu$ (where ν is the kinematic viscosity) and Weber number $W = \rho g h_o^2/\sigma$ (where ρ is the density and σ is the surface tension of water) were calculated for all models with $0.38 < h_o/P < 1.04$. Both Reynolds and Froude numbers were within the range of previous laboratory experiments indicating that the proposed laboratory tests were scalable [5,24]. Empirical correlations for prediction of discharge coefficient of sharp-crested weirs can be formulated for very low flow where the effect of surface tension becomes important. In this study, the effect of surface tension accounts for 0.72% of the discharge coefficient in the lowest discharge of 3.82 L/s using Rehbock's formulations [1]. Three downstream conditions of free, modular limit, and submerged flow were tested in this study. Fig. 4 shows the side view images of the water surface over half-cosine sharp-crested weirs with the top width ratio of w/b = 1/7 and 1/4 in free, modular limit, and submerged flow conditions. The modular limit condition for w/b = 1/7 and 1/4 occurred at t/h = 0.166 and 0.12, respectively.

The instantaneous three-dimensional water velocity components and turbulent characteristics were measured along x (longitudinal), y (vertical), and z (transverse) directions, respectively. An Acoustic Doppler Velocimeter ADV (Vectrino, Nortek AS, Norway) was used for flow measurements at a cross section 20 mm upstream of the weirs, as shown in Fig. 2. The sampling volume of the ADV probe was a cylinder with a height of 5 mm and a fixed diameter of 6 mm measuring time series water velocity 50 mm further away from the ADV probe. Cumulative averaging method was employed to determine the sampling duration [22]. It was found that a sampling duration of 120 s at a sampling rate of 200 Hz can provide steady flow measurements with cumulative velocity fluctuations in the range of ± 5%. In addition, great care was taken to filter data with a correlation coefficient below 0.7 and a signal-to-noise ratio less than 15 to ensure high quality measurements [19,31].

4. Experimental results and discussion

4.1. Mean flow velocity

Variations of the mean water velocities of contracted rectangular and half-cosine sharp-crested weirs in three directions of streamwise v_x, vertical v_y, and transverse v_z are plotted in Figs. 5–7. The y-z plane for velocity measurement is located 20 mm upstream of the weir models. Mean velocities are normalized with the average water velocity in the y-z plane v_{ave}. The vertical position y is normalized with the vertical distance from the crest to the top end of the weir D, and the transverse position z is normalized with the crest width of the weirs b (see Fig. 2a). Based on the position of origin (see Fig. 2) the average water velocities are measured below and above the crest elevation indicating negative and positive values for y ranging from $-0.3 \le y/D \le 0.23$.

Fig. 5 shows the variations of the normalized streamwise velocity in y-z plane. As can be seen, the normalized streamwise velocity is constant along the z axis and below the crest elevation for all types of weirs with a maximum value of v_x/v_{ave} ranging from 0.5 to 0.6. The maximum streamwise velocity occurs at the crest elevation (i.e., y/D = 0). Our observation is consistent with the laboratory observations of Rajaratnam and Muralidhar [29] on full width sharp-crested weirs. At the crest elevation (i.e., y/D = 0), the magnitude of v_x depends on the shape of the weir and v_x significantly decreases in transverse direction.

Table 1
Geometries and flow characteristics of half-cosine and rectangular sharp-crested weirs.

Weir model	w (mm)	b (mm)	P (mm)	w/b	h_o (mm)	Q_f (L/s)	h_o/P	F	R ($\times 10^3$)	W
1	0	180	130	0	50	3.82	0.38	0.089	35	337
					75	6.68	0.58	0.128	64	759
					100	9.59	0.77	0.154	99	1348
					125	12.26	0.96	0.169	138	2107
					150	14.38	1.15	0.172	182	3034
2	0	180	180	0	55	4.51	0.31	0.070	40	408
					68	5.94	0.38	0.085	56	624
					75	6.93	0.42	0.095	64	759
					80	7.63	0.44	0.102	71	863
					90	9.01	0.50	0.114	85	1092
					95	9.47	0.53	0.116	92	1217
					105	10.39	0.58	0.121	107	1487
					115	11.00	0.64	0.122	122	1783
					126	11.87	0.70	0.124	140	2141
					138	13.08	0.77	0.129	161	2568
3	0	180	230	0	48	4.51	0.21	0.055	33	311
					61	5.94	0.27	0.067	47	502
					68	6.93	0.30	0.076	56	624
					75	7.63	0.33	0.080	64	759
					84	9.01	0.37	0.091	76	951
					88	9.47	0.38	0.094	82	1044
					101	10.39	0.44	0.097	101	1376
					112	11.00	0.49	0.098	117	1692
					123	11.87	0.53	0.100	135	2040
					135	13.08	0.59	0.105	155	2458
					149	14.17	0.65	0.108	180	2994
4	30	210	130	1/7	50	4.95	0.38	0.099	35	337
					75	8.31	0.58	0.136	64	759
					100	11.23	0.77	0.155	99	1348
					125	14.38	0.96	0.170	138	2107
					150	16.51	1.15	0.169	182	3034
5	30	210	180	1/7	42	4.51	0.23	0.065	27	238
					52	5.94	0.29	0.081	37	365
					57	6.93	0.32	0.091	43	438
					62	7.63	0.34	0.097	48	518
					70	9.01	0.39	0.110	58	661
					76	9.47	0.42	0.111	66	779
					80	10.39	0.44	0.119	71	863
					88	11.00	0.49	0.121	82	1044
					95	11.87	0.53	0.125	92	1217
					102	13.08	0.57	0.133	102	1403
					110	14.17	0.61	0.138	114	1632
					117	14.72	0.65	0.138	125	1846
					124	15.33	0.69	0.139	137	2073
					131	15.58	0.73	0.137	149	2314
					139	16.48	0.77	0.139	162	2605
					146	17.73	0.81	0.145	175	2874
6	30	210	230	1/7	42	4.51	0.18	0.048	27	238
					51	5.94	0.22	0.061	36	351
					57	6.93	0.25	0.068	43	438
					63	7.63	0.27	0.073	50	535
					70	9.01	0.30	0.083	58	661
					73	9.47	0.32	0.086	62	719
					79	10.39	0.34	0.092	70	842
					88	11.00	0.38	0.093	82	1044
					96	11.87	0.42	0.097	93	1243
					103	13.08	0.45	0.103	104	1431
					112	14.17	0.49	0.108	117	1692
					119	14.72	0.52	0.109	129	1910
					127	15.33	0.55	0.109	142	2175
					132	15.58	0.57	0.109	150	2350
					142	16.48	0.62	0.110	168	2719
					150	17.73	0.65	0.115	182	3034

(*continued on next page*)

Table 1 (*continued*)

Weir model	w (*mm*)	b (*mm*)	P (*mm*)	w/b	h_o (*mm*)	Q_f (*L/s*)	h_o/P	F	R ($\times 10^3$)	W
7	60	240	130	1/4	50	6.56	0.38	0.114	35	337
					75	10.39	0.58	0.149	64	759
					100	14.22	0.77	0.172	99	1348
					125	18.70	0.96	0.193	138	2107
					150	20.78	1.15	0.187	182	3034
8	60	240	180	1/4	38	4.51	0.21	0.059	23	195
					47	5.94	0.26	0.073	32	298
					53	6.93	0.29	0.082	38	379
					57	7.63	0.32	0.088	43	438
					63	9.01	0.35	0.100	50	535
					66	9.47	0.37	0.103	53	587
					73	10.39	0.41	0.109	62	719
					78	11.00	0.43	0.112	68	820
					85	11.87	0.47	0.116	78	974
					90	13.08	0.50	0.124	85	1092
					95.5	14.17	0.53	0.130	92	1230
					100	14.72	0.56	0.132	99	1348
					105	15.33	0.58	0.134	107	1487
					111.5	15.58	0.62	0.132	117	1676
					117.5	16.48	0.65	0.135	126	1862
					121	17.73	0.67	0.143	132	1974
					126	18.02	0.70	0.142	140	2141
					132.5	18.89	0.74	0.144	151	2367
					137	19.34	0.76	0.144	159	2531
					141.5	19.79	0.79	0.144	167	2700
					145	20.94	0.81	0.150	173	2835
9	60	240	230	1/4	40	4.51	0.17	0.043	25	216
					45	5.94	0.20	0.055	30	273
					53	6.93	0.23	0.061	38	379
					57	7.63	0.25	0.066	43	438
					64	9.01	0.28	0.075	51	552
					67	9.47	0.29	0.078	54	605
					74	10.39	0.32	0.082	63	738
					79	11.00	0.34	0.085	70	842
					85	11.87	0.37	0.089	78	974
					91	13.08	0.40	0.096	86	1117
					96	14.17	0.42	0.101	93	1243
					100	14.72	0.43	0.103	99	1348
					105	15.33	0.46	0.105	107	1487
					111	15.58	0.48	0.104	116	1661
					117	16.48	0.51	0.107	125	1846
					121	17.73	0.53	0.113	132	1974
					126	18.02	0.55	0.113	140	2141
					132	18.89	0.57	0.115	150	2350
					137	19.34	0.60	0.116	159	2531
					141	19.79	0.61	0.116	166	2681
					146	20.94	0.63	0.121	175	2874
10	SCW	180	130	–	35–150	3.82–21.64	0.33–1.12	0.013–0.21	53–150	398–1878
11	SCW	180	180	–	35–150	3.82–21.64	0.33–1.12	0.013–0.21	53–150	398–1878
12	SCW	180	230	–	35–150	3.82–21.64	0.33–1.12	0.013–0.21	53–150	398–1878

The maximum velocities for half-cosine weirs with $w/b = 0$, 1/7, and 1/4 at $y/D = 0$ and $z/b = 0$ are 1.84, 1.57, and 1.44 times of the average velocity in y-z plane, respectively. Whereas this value for contracted rectangular weir is 1.3. Considering the fact that the flow rates in all weirs are similar, the high values of streamwise velocity in half-cosine weirs indicate strong shear layer formation and high degree of energy dissipation as shown in Fig. 5.

In general, the mean velocities in y and z directions represent the formation of secondary currents that are perpendicular to the main flow direction. Secondary currents can be generated and enhanced due to many factors such as development of strong shear layer, streamline curvature, anisotropy of turbulence, and centrifugal forces. Variations of the normalized vertical velocity with the normalized transvers distance from the origin and at different depth are shown in Fig. 6. At 20 mm upstream of the weir, all vertical velocity components are positive for rectangular weir indicating that at this position water parcels react to the change of flow stream due to presence of weir structure but, water parcels do not fall over the weir. Fig. 6a shows a significant change in the vertical velocity profiles in comparison with the velocity profiles of rectangular weirs. As can be seen, the vertical component of water velocity is negative above the crest indicating that the water parcels follow the streamline and they are about to flow over the weir. The difference on the vertical velocity profiles of the half-cosine and rectangular weirs may be due to the three-dimensional velocity pattern in half-cosine weirs. Similar vertical velocity pattern in y-z plane was reported for sinusoidal sharp-crested weirs [19].

Fig. 7 shows the variations of the water velocity in transverse direction for both rectangular and half-cosine weirs at different normalized depths. As can be seen, the water velocity in transverse direction is zero at the centerline of the weir and it is almost constant below the weir crest at $y/D = -0.3$ indicating a two-dimensional flow at this level. However, the transverse component of water velocity increases close and above the weir crest showing a strong three-dimensional flow especially for $0.25 < z/b < 0.5$. As can be seen from Fig. 7, the peak

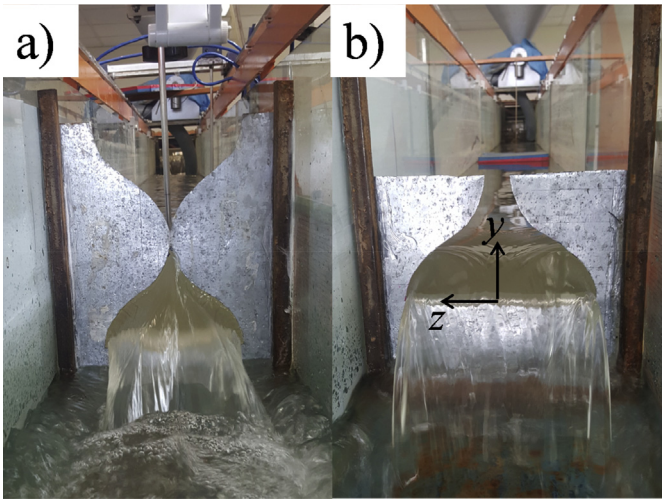

Fig. 3. Front view images of cosine sharp-crested weirs in free flow conditions; a) $w/b = 0$, $Q_f = 14.8$ L/s; b) $w/b = 1/7$, $Q_f = 8.12$ L/s.

transverse velocity for half-cosine weirs occurred close to the water surface at $y/D = 0.23$ with a value of $v_z/v_{ave} \approx 0.5$ whereas for contracted rectangular weir model (Fig. 7d), the peak transverse velocity occurred at the crest level (i.e., $y/D = 0$) due to interaction of lower nappe with the weir plate. This clearly shows that the wall effect on half-cosine weirs results in formation of three-dimensional flow. Close to water surface at $y/D = 0.23$, the location of the peak transverse velocity for half-cosine weirs is at $z/b = 0.146$ whereas for rectangular sharp-crested weir the location of the peak transverse velocity moves toward the wall to $z/b = 0.29$.

4.2. Turbulent characteristics

The streamwise, vertical and transverse water velocity fluctuations for half-cosine and rectangular weirs were calculated from the instantaneous time-series velocity measurements. For half-cosine and rectangular weirs the turbulent intensities at 20 mm upstream of the weir in streamwise and vertical directions were around 10% of the averaged mean velocity v_{ave} whereas in transverse direction v_z' was around 5% of v_{ave}. The magnitude of the streamwise and transverse velocity fluctuations increased toward the edge of the weir models. In order to study the distribution of velocity fluctuations in the upstream of the weir structure at $x = -20$ mm, contour plots of the vertical, and transverse velocity fluctuations in y-z plane for both half-cosine $w/b = 0$ and rectangular weirs were developed from the ADV measurements. It was found that the streamwise velocity fluctuations for half-cosine and rectangular weirs are somewhat similar so they were excluded from Fig. 8. As can be seen, the root-mean-square (i.e., rms) velocity fluctuations in vertical direction v_y' for half-cosine weir were well distributed around the weir structure whereas high velocity fluctuation was observed at the sides and bottom of the rectangular weir. In contrary, transverse velocity fluctuations became significant on half-cosine weir due to sudden transverse velocity acceleration and strong shear layer formation due to boundary effect.

Turbulent kinetic energy is an average of velocity fluctuations at three main directions [32] which can be normalized with v_{ave} as

$$T = \frac{(v_x'^2 + v_y'^2 + v_z'^2)^{1/2}}{3v_{ave}} \tag{11}$$

Excluding the streamwise direction, the main contribution of the turbulent kinetic energy for half-cosine weirs is from transverse direction whereas for rectangular weirs, both vertical and transverse directions contribute to the turbulent kinetic energy.

Fig. 9 shows the variations of the turbulent kinetic energy in y-z plane 20 mm upstream of the weir structure. As can be seen, the turbulent kinetic energy has higher values for half-cosine weirs at the bottom of the channel (i.e., $y/D = -0.3$) in comparison with rectangular sharp-crested weir. This is due to the strong values of v_z' at the edge of the weir structure (see Fig. 8a). Higher values of turbulent kinetic energy in the lower depths for half-cosine weirs make these types of weirs capable of sediment resuspension and sediment removal. A sudden drop of turbulent kinetic energy at $z/b = 0.15$ also indicated the existence of a strong stream flow with small flow disturbance which results in higher mean flow energy. This high mean flow energy was also observed as a peak mean flow in transverse direction as described in Fig. 7a and c. Our laboratory experiments indicated that the average turbulent kinetic energy over y-z plane for half-cosine sharp-crested weir was approximately 19.2% higher than that of rectangular weir of the same conditions. This difference was 15% between one-cycle

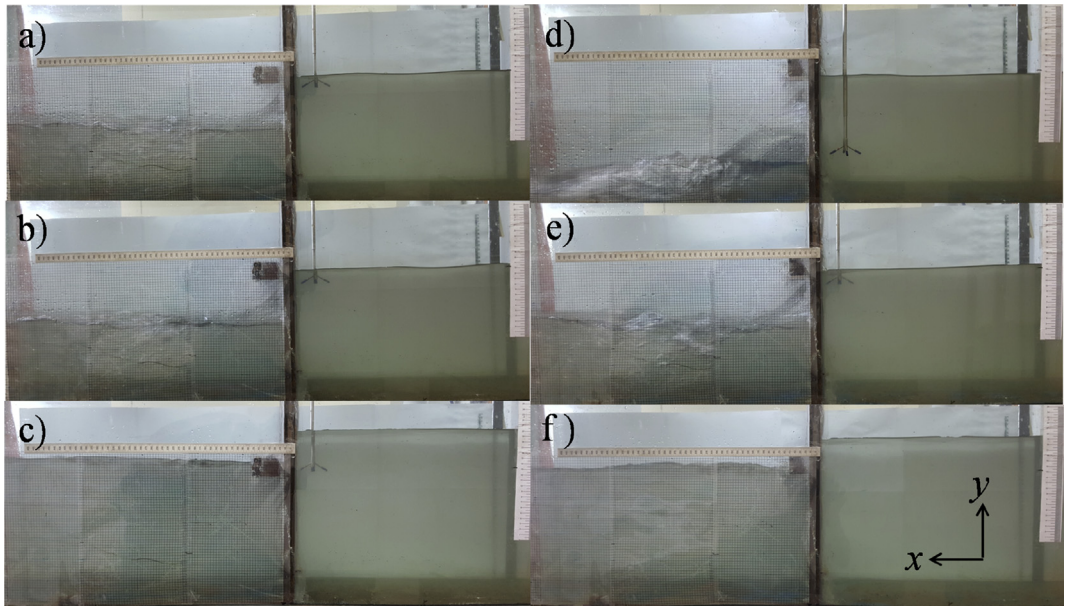

Fig. 4. Water surface profiles of cosine sharp-crested weirs in different flow conditions for $Q_f = 8.12$ L/s; a) $w/b = 1/7$, free flow; b) $w/b = 1/7$, modular limit ($t/h = 0.166$); c) $w/b = 1/7$, submerged flow, $t/h = 0.87$; d) $w/b = 1/4$, free flow; e) $w/b = 1/4$, modular limit ($t/h = 0.12$); e) $w/b = 1/4$, submerged flow, $t/h = 0.86$.

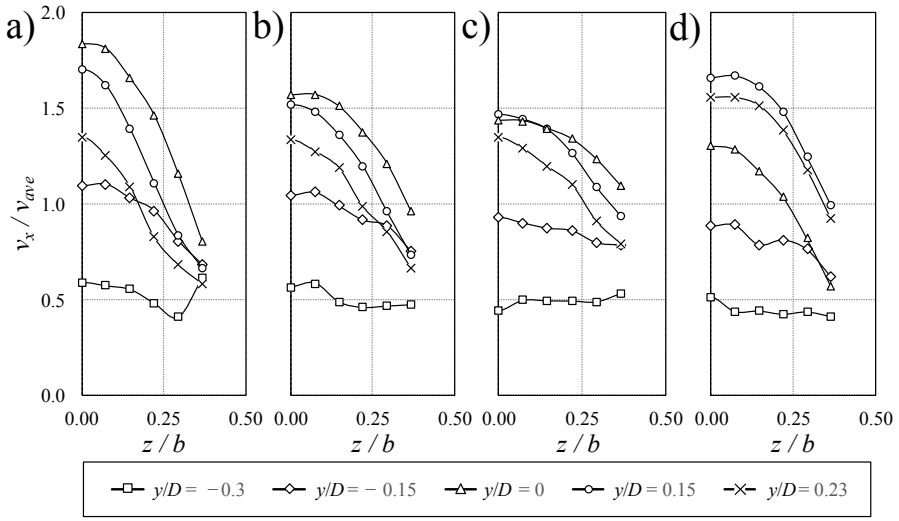

Fig. 5. Variations of the normalized streamwise velocity with the normalized distance from the centreline of the weirs at different depths; a) half-cosine weir $w/b = 0$; b) half-cosine weir $w/b = 1/7$; c) half-cosine weir $w/b = 1/4$; d) sharp-crested rectangular weir.

sinusoidal and contracted rectangular sharp-crested weirs [19].

4.3. Head-discharge relationship

The head-discharge relationship for half-cosine sharp-crested weirs can be formulated by using Bernoulli's equation and neglecting the approach velocity head [2]. The velocity of water at any arbitrary point upstream of the weir can be described by

$$v_w = C_d\sqrt{2g(h_o - y)} \tag{12}$$

where y is defined as the water height above the crest level (see Fig. 2b). For half-cosine weir sections, the width of the weir can be defined knowing the cosine magnifying factor S (see Fig. 1). The magnifying factor is defined as a parameter to determine the weir cross-section area and for cosine weirs $S = b_a$. Therefore, a cosine weir of a larger size can be adopted to the weir equation by changing the magnifying factor. The width of the weir b at any flow depth y can be determined as

$$b = w + 2b_a \cos\left(\frac{2\pi n y}{D}\right) \tag{13}$$

The total flow rate in free flow condition can be calculated using continuity equation as

$$Q_f = \int_0^{h_o} v_w b dy = \int_0^{h_o} C_d\sqrt{2g(h_o - y)}\left[w + 2b_a \cos\left(\frac{2\pi n y}{D}\right)\right] dy \tag{14}$$

The integration in Eq. (14) can be numerically solved using Fresnel integrals by Maple software (Maple soft ver. 18, Canada). The solution of the continuity equation using Fresnel integrals can be described as

$$Q_f = \frac{2\sqrt{2g}\,C_d}{(2\pi n/D)^{3/2}}\left[13w\left(\frac{2\pi n h_o}{D}\right)^{3/2} + b\left(\frac{2\pi n h_o}{D}\right)^{1/2} + b_a\sqrt{\frac{\pi}{2}}\left[\begin{matrix}\sin\left(\frac{2\pi n h_o}{D}\right)C_1\left(\frac{4nh_o}{D}\right)^{1/2} \\ + \cos\left(\frac{2\pi n h_o}{D}\right)^{1/2} + C_2\left(\frac{4nh_o}{D}\right)\end{matrix}\right]\right] \tag{15}$$

The integral constants of C_1 and C_2 are very small and they are in the range of $0 \le C_1 \le 0.0001$ $(D/4nh_o)$ and -0.002 $(D/4nh_o)$ $\le C_2 \le 0.002$ $(D/4nh_o)$. Assuming uniform velocity distribution over the weir and neglecting the minimal effects of C_1 and C_2, Eq. (15)

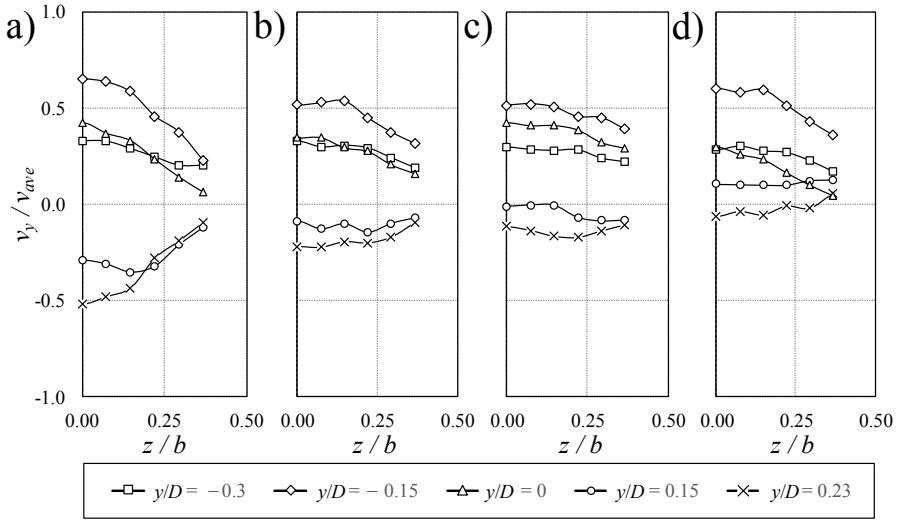

Fig. 6. Variations of the normalized vertical velocity with the normalized distance from the centreline of the weirs at different depths; a) half-cosine weir $w/b = 0$; b) half-cosine weir $w/b = 1/7$; c) half-cosine weir $w/b = 1/4$; d) sharp-crested rectangular weir.

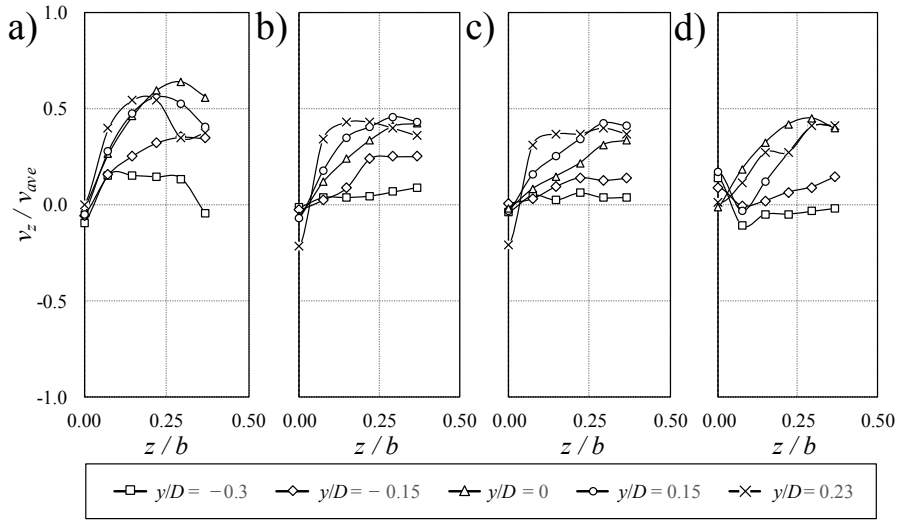

Fig. 7. Variations of the normalized transverse velocity with the normalized distance from the centreline of the weirs at different depths; a) half-cosine weir $w/b = 0$; b) half-cosine weir $w/b = 1/7$; c) half-cosine weir $w/b = 1/4$; d) sharp-crested rectangular weir.

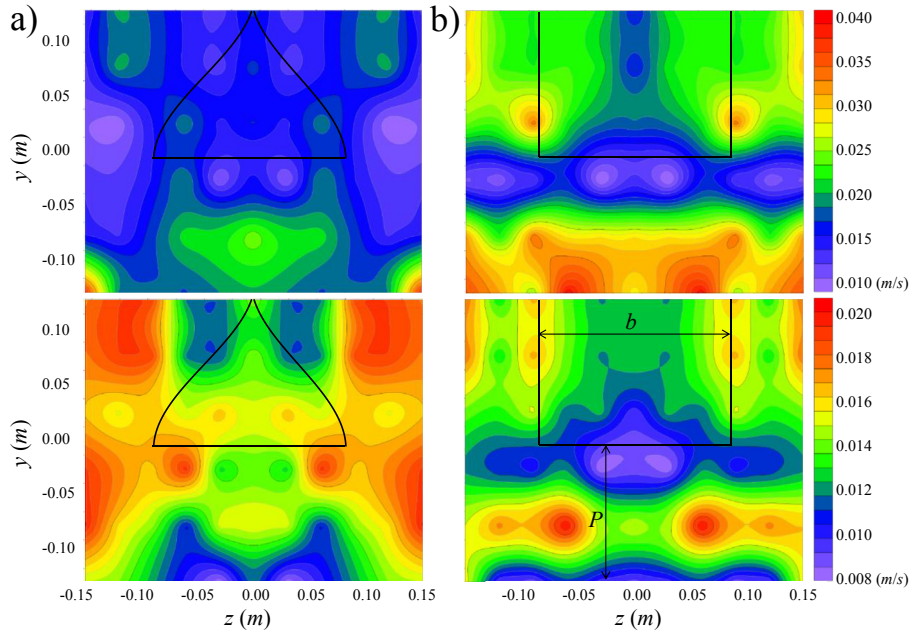

Fig. 8. Contour plots of the vertical v_y' (top), and transverse v_z' (bottom) velocity fluctuations for half-cosine and sharp-crested weirs in free flow condition; a) half-cosine weir $w/b = 0$, $h_o = 135$ mm, $Q_f = 14.38$ (L/s); b) sharp-crested rectangular weir, $h_o = 135$ mm, $Q_f = 21.6$ (L/s).

simplified to as

$$Q_f = \frac{2\sqrt{2g}\,C_D}{(2\pi n/D)^{3/2}}\left[13w\left(\frac{2\pi n h_o}{D}\right)^{3/2} + b\left(\frac{2\pi n h_o}{D}\right)^{1/2}\right] \quad (16)$$

where C_D is the discharge coefficient calculated by the approximated relationship.

4.4. Discharge characteristics

Fig. 10 shows the variations of the discharge coefficient of half-cosine weirs with different weir top widths w and rectangular contracted sharp-crested weirs. Discharge coefficient can be either calculated using continuity equation and determining the Fresnel integrals C_d or using the proposed head-discharge relationship using Eq. (16). Variations of discharge coefficient C_d for half-cycle cosine weirs with h_o/P is shown in Fig. 10a. As can be seen, the value of discharge coefficient based on continuity equation and solving Fresnel integrals C_d decreases almost linearly with h_o/P due to the geometry of half-cosine weirs since the weir's width decreases as the water head rises. In addition, the gap between the cosine plates increase the opening area of the weir and this increases the flow rate for half-cosine weirs of wider top width (i.e., $w/b = 1/4$) with the same water head. It is not practical to solve the Fresnel integrals to estimate flow discharge in a daily basis. Therefore, it is beneficial to use the head-discharge equation developed by solving the Fresnel integrals (Eq. (16)) and find a correlation between the discharge coefficient C_D and the weir geometry. Fig. 10b shows the correlation of C_D with h_o/P for contracted rectangular and half-cosine weirs with different top widths. Semi-empirical equations to predict full-width, and contracted rectangular sharp-crested weirs are also added for comparison. In contrast with rectangular sharp-crested weirs where C_D increases with h_o/P due to complete formation of nappe, C_D in half-cosine weirs decreases with h_o/P due to change of

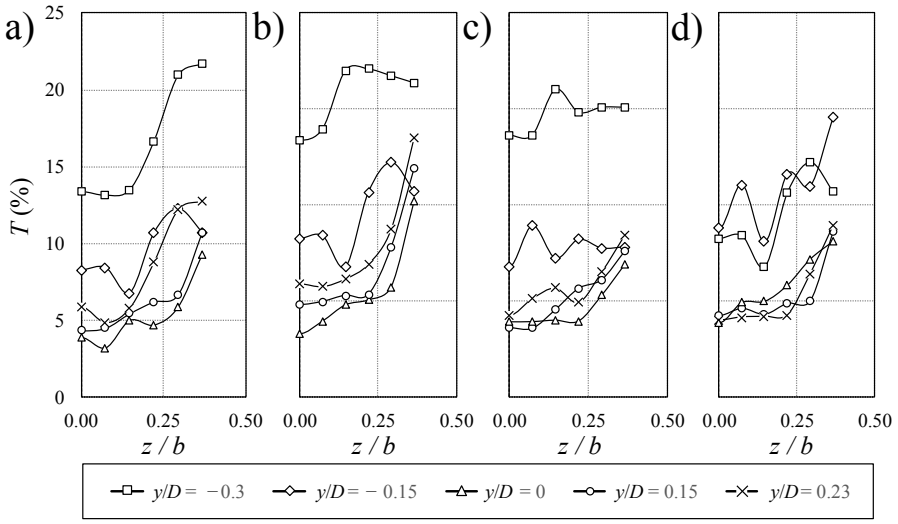

Fig. 9. Variations of the normalized turbulent kinetic energy with the normalized distance from the centreline of the weirs at different depths; a) half-cosine weir $w/b = 0$; b) half-cosine weir $w/b = 1/7$; c) half-cosine weir $w/b = 1/4$; d) sharp-crested rectangular weir.

weir's width with h_o. The advantage of using half-cosine weirs over rectangular weirs is that half-cosine weirs are more sensitive to high flow rates due to the geometry of the weir and they show higher water head changes with small changes in discharge. Considering the effective parameters on variations of discharge coefficient, an empirical formulation is developed to describe the variation of C_D with the weir parameters as

$$C_D = 0.28\left(\frac{h_o}{P}\right)^2 - 0.56\left(\frac{h_o}{P}\right) + 0.11\left(\frac{w}{b}\right) + 0.667 \tag{17}$$

Dotted curves in Fig. 10b shows the performance of the proposed formulation for prediction of discharge coefficient of half-cosine weirs for $w/b = 0$, 1/7, and 1/4 with a regression coefficient of $R^2 = 0.81$. Fig. 10c shows the comparison between the discharge coefficients based on the two approaches. The discharge coefficient predicted by Eq. (17) is on average 5.5% smaller than the measured discharge coefficient C_d. Performance of the head-discharge formulations based on continuity equation and solving the Fresnel integrals and the proposed head-discharge equation (Eq. (17)) is shown in Fig. 11. This figure shows the variations of the predicted flow discharge ratio with h_o/P. As can be seen, the variations of the discharge are within around ± 10%. Data scatter in prediction of discharge coefficients and discharges are due to a number of reasons such as presence of three-dimensional flow near the weir structure, non-uniform velocity distribution, uncertainty of head and discharge measurements, truncation of Fresnel integrals to develop a simpler and more practical equation (Eq. (16)), and data scatter in the regression analysis with an R^2 value of 0.81.

Fig. 12a shows the correlation of headwater and tailwater in submerged flow condition for weir models with the weir heights of $P = 0.13$ m, 0.18 m and 0.23 m. As can be seen, the normalized headwater h/P is constant for $t/P \leq 0.3$ which indicates that for the submergence threshold of $t/P > 0.3$, all types of weirs including contracted rectangular weir show a linear correlation with a constant slope. The correlation between the head and the tailwater for half-cosine weirs with $w/b = 0$ indicates a linear correlation with a same slope for both intermediate (i.e., $0.6 < t/h < 0.8$) and deeply (i.e., $t/h \geq 0.8$) submerged flow. However, the slope of correlation for other values of w/b significantly increases at a certain t/P. For instance, for rectangular sharp-crested weir the sudden slope change occurs at $t/P = 0.61$ corresponding to $t/h = 0.55$. This indicates that for $t/P > 0.61$, a slight change in the tailwater level causes a significant change in the headwater due to change in the slope of correlation. The threshold values of t/P for slope change in Fig. 12a for half-cosine weirs with $w/b = 0$, 1/7, and 1/4 are 1.3, 1.02, and 0.8, respectively. The stability of weir performance in the intermediate submergence is very important and significant headwater raise due to tailwater change is undesirable for flow control. Fig. 12a clearly shows that half-cosine weirs are less sensitive to tailwater variations in mid-range of submergence (i.e., $0.6 < t/h < 0.8$).

Performance of weirs in submerged flow condition can be evaluated by considering the variations of discharge reduction factor ψ from Eq. (4) and submergence t/h. Fig. 12b shows the correlations of ψ with t/h for triangular labyrinth weir (TLW), contracted rectangular, and half-cosine sharp-crested weirs (SCW). The discharge reduction curves from experimental study of Bijankhan and Kouchakzadeh [30] for triangular labyrinth weirs (TLW), Abou-Seida and Quraishi [6] for full width sharp-crested weir (SCW) and proposed formulation of Wu and Rajaratnam [21] for deeply submerged full width sharp-crested weirs are also included for comparison. As can be seen, contracted sharp-crested weirs in general are more sensitive than the full width sharp-crested weirs due to limited contact area between upstream and downstream sections. In addition, flow discharge significantly reduces for high submergence in half-cosine weirs which makes these types of weirs less desirable in submerged flow condition. On the other hand, triangular labyrinth weirs showed a lower sensitivity in submerged flow condition in comparison with sharp-crested weirs. For example, for constant submergence level $t/h = 0.8$, half-cosine weirs can only pass around 40% of the corresponding flow discharge in free flow condition for each weir type (i.e., $0.4Q_f$) whereas at the same submergence level, contracted and full width rectangular weirs can pass around $0.58Q_f$ and $0.7Q_f$, respectively. It worth noting that at $t/h = 0.8$, triangular labyrinth weirs can pass $0.85Q_f$. Therefore, despite the fact that half-cosine weirs are less sensitive for tailwater variations in the mid-range of submergence, but they are more sensitive for operation in submerged flow condition if flow passage being considered as a key factor.

An empirical formulation was developed for prediction of contracted rectangular sharp-crested weir (SCW) based on laboratory data as

$$\psi = \frac{(1/3)^{2/5}\sqrt{1-(t/h)^4}}{[0.605 + 0.08(h_o/P)]} \tag{18}$$

A solid curve shows the proposed equation in Fig. 12b. Our observations in submerged flow condition indicated that the weir top width w in the range being tested doesn't change the performance of the weir in submerged flow condition and the discharge reduction factor decreases linearly with t/h. A solid line in Fig. 12b shows the

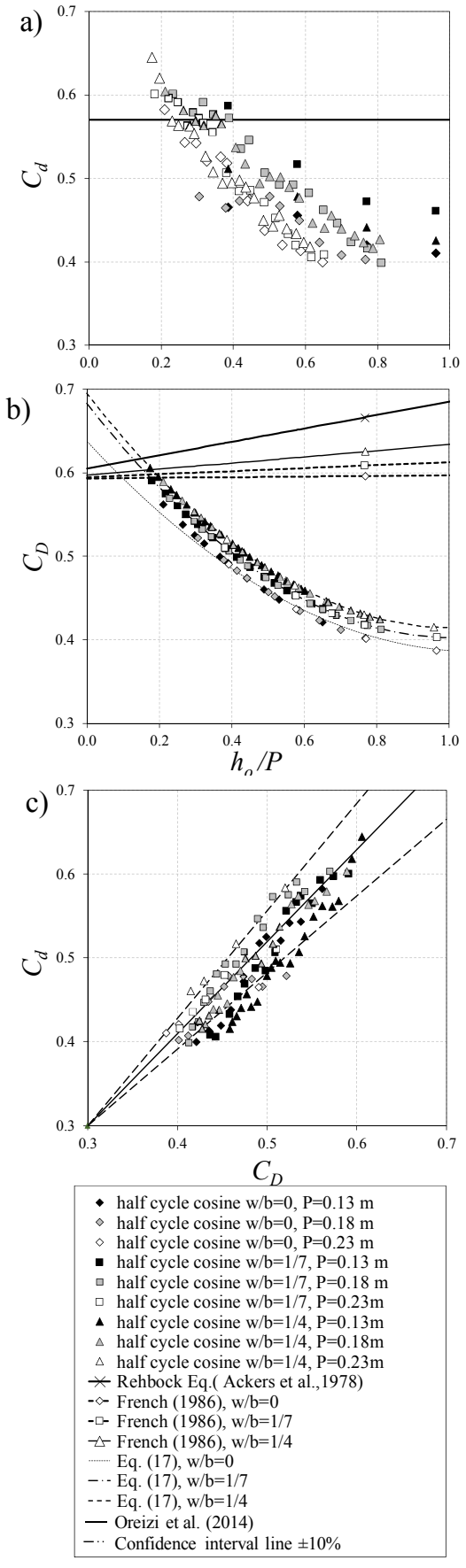

Fig. 10. Variations of the discharge coefficient of cosine sharp-crested weirs with h_o/P; a) discharge coefficient based on flow rate with constant velocity and solving Fresnel integrals C_d; b) discharge coefficient based on the proposed head-discharge relationship for cosine sharp-crested weir C_D; c) comparison between C_d and C_D.

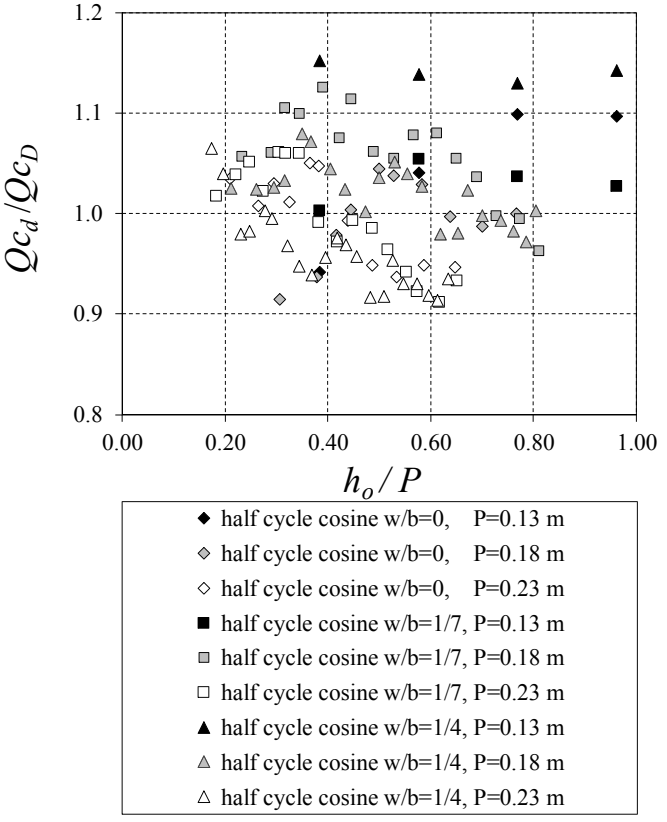

Fig. 11. Performance of the head-discharge equations for half-cosine sharp-crested weirs based flowrate with constant velocity and solving Fresnel integrals (C_d) and the proposed head-discharge equation (Eq. (17)) to predict C_D.

correlation of half-cosine sharp-crested weirs with submergence and it can be formulated as

$$\psi = \frac{3}{2}\left(1 - \frac{t}{h}\right) \tag{19}$$

5. Conclusions

This study presents a detailed analysis of half-cosine sharp-crested weirs with different weir heights and top width openings in both free and submerged flow conditions. Detailed velocity measurements in streamwise, vertical, and transverse directions were conducted in a *y-z* plane 20 mm upstream of the weir models. Turbulent characteristics such as turbulent fluctuations and turbulent kinetic energy were calculated using instantaneous time-series velocity data. The head-discharge coefficient was theoretically developed for half-cycle cosine weirs and the Fresnel integral was solved numerically. A formula was also developed to estimate discharge for practical purposes. Effect of tailwater level on performance of contracted rectangular and half-cosine sharp-crested weirs was investigated and the discharge reduction factor was correlated with the submergence level for both weir types. It was found that the half-cosine weirs are less sensitive to tailwater variations in mid-range of submergence (i.e., $0.6 < t/h < 0.8$).

Three dimensional velocity data was analyzed to identify the magnitude and location of secondary currents. It was observed that the

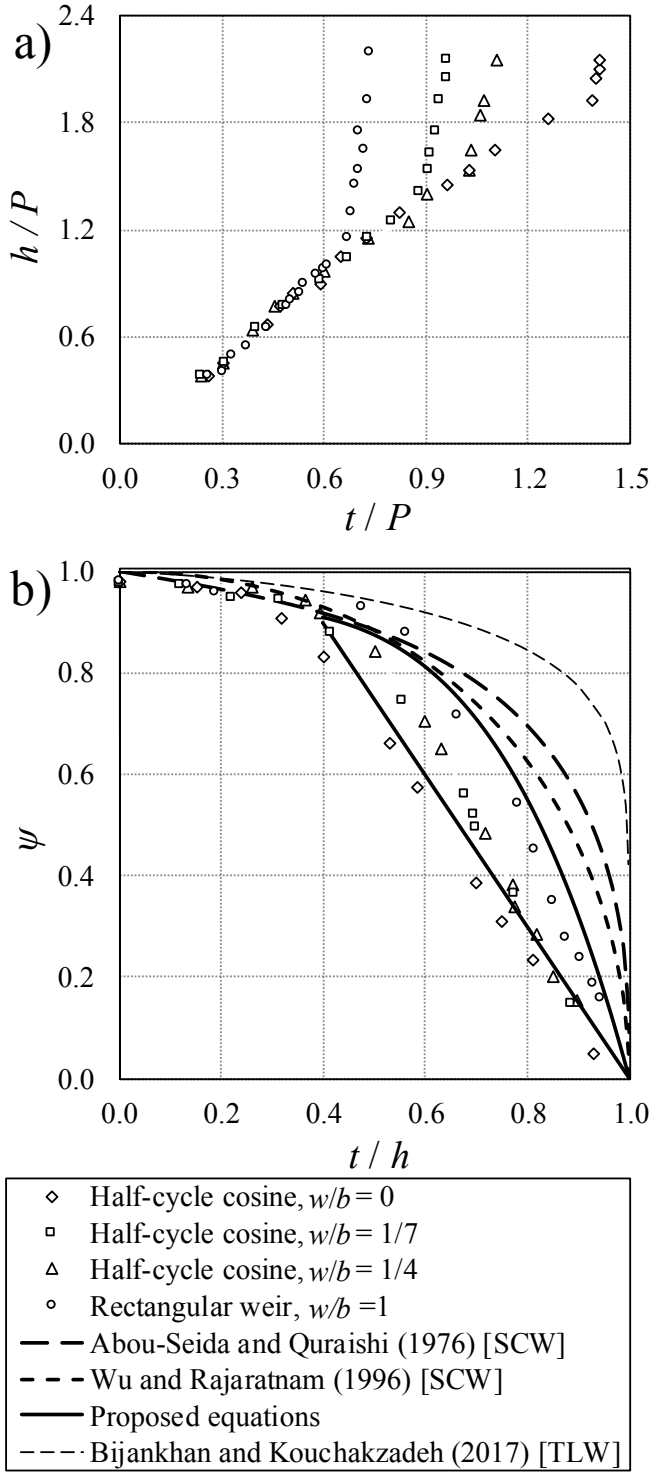

Fig. 12. Performance of half-cosine sharp-crested weirs in submerged flow condition; a) variations of the normalized head water with t/P in submerged flow condition; b) variations of the discharge reduction factor ψ with submergence t/h.

maximum streamwise velocity at the crest elevation depends upon the shape of the weir and it was ranging from 1.44 to 1.84 times of the averaged velocity for half-cosine weirs and $1.3v_{ave}$ for rectangular sharp-crested weirs. The water velocity in transverse direction showed a strong three-dimensional flow for $0.25 < z/b < 0.5$. The location of the peak transverse velocity for half-cosine weirs is at $z/b = 0.146$ whereas for rectangular sharp-crested weirs it moves toward the wall to $z/b = 0.29$. It was found that the streamwise velocity fluctuations for both half-cosine and rectangular weirs are similar and the differences on the turbulent structure were due to the vertical and transverse velocity fluctuations. In addition, transverse velocity fluctuations became a significant contributor of turbulent kinetic energy for half-cosine weirs due to sudden transverse velocity acceleration and strong shear layer formation.

It was found that the regions of the highest turbulence intensity were near the walls for both half-cosine and rectangular weirs and the location of highest turbulent intensity decreased toward the middle of weir model. The higher values of the turbulent kinetic energy at the lower depths of half-cosine weirs makes them capable of sediment resuspension and sediment removal. Our laboratory experiments indicated that the average turbulent intensity for half-cosine sharp-crested weir is approximately 19.2% higher than that of rectangular weir of the same conditions whereas this difference for one-cycle sinusoidal weirs was 15%.

Notation

The following symbols are used in this paper

A	channel cross-sectional area
B	weir length
b_a	amplitude of the cosine wave
B	channel width
C_1	integral constant
C_2	integral constant
C_d	coefficient of discharge for free flow condition (theoretical)
C_D	coefficient of discharge for free flow condition (practical)
D	distance from the weir crest to the weir top
F	Froude number
g =	gravity acceleration
h	head on weir
h_o	head on upstream weir for free flow condition
n	cycle number
P	height of weir
Q	flow discharge
R	Reynolds number
S	magnifying factor
t	depth of tailwater above crest
T	turbulent kinetic energy
v	velocity
v'	velocity fluctuation
w	weir top width
W	Weber number
y	vertical distance from the weir crest
α	energy coefficient
β	momentum coefficient
ν	kinematic viscosity
ρ	density of water
σ	Surface tension
ψ	discharge reduction factor for submerged flows

Subscripts

ave	average; and
e	effective
f	free flow
s	submerged flow
w	water
x	streamwise direction
y	vertical direction
z	transverse direction

Appendix A. Supplementary data

Supplementary data to this article can be found online at https://doi.org/10.1016/j.flowmeasinst.2019.02.002.

References

[1] P. Ackers, W.R. White, J.A. Perkins, A.J. Harrison, Weirs and Flumes for Flow Measurement, John Wiley & Sons Ltd, Chichester, West Sussex, UK, 1978, p. 327.
[2] M.G. Bos, Discharge Measurement Structure, third ed., international Institute for Land Reclamation and Improvement, Wageningen, The Netherlands, 1989, p. 394.
[3] A.H. Azimi, N. Rajaratnam, Discharge characteristics of weirs of finite crest length, J. Hydraul. Eng. 135 (12) (2009) 1081–1085.
[4] W.H.H. Banks, C.R. Burch, T.L. Shaw, The design of proportional and logarithmic thin-plate weirs, J. Hydraul. Res. 6 (2) (1968) 75–106.
[5] P.K. Swamee, S.K. Pathak, M. Ghodsian, Viscosity and surface tension effects on rectangular weirs, The ISH Journal of Hydraulic Engineering 7 (2) (2001) 45–50.
[6] M.M. Abou-seida, A.A. Quraishi, A flow equation for submerged rectangular weirs, Proc. Instn. Civ. Engrs, Part 2 61 (4) (1976) 685–696.
[7] C. Igathinathane, I. Srikanth, K. Prakash, B. Ramesh, A.R. Womac, Development of parabolic weirs for simplified discharge measurement, J. Biosyst. Eng. 96 (1) (2007) 111–119.
[8] R. Baddour, Head-discharge equation for sharp-crested polynomial weir, J. Irrigat. Drain. Eng. 134 (2) (2008) 260–262.
[9] A.R. Vatankhah, Flow measurement using circular sharp-crested weirs, Flow Meas. Instrum. 21 (2010) 118–122.
[10] M. Bijankhan, V. Ferro, Assessing stage-discharge relationships for circular overflow structure, J. Irrigat. Drain. Eng. (2017), https://doi.org/10.1061/(ASCE)IR.1943-4774.0001246.
[11] C. Di Stefano, V. Ferro, M. Bijankhan, New theoretical solution of the outflow process for a weir with complex shape, J. Irrigat. Drain. Eng. (2016), https://doi.org/10.1061/(ASCE)IR.1943-4774.0001045.
[12] A.R. Vatankhah, Head-discharge equation for sharp-crested weir with piecewise-linear sides, J. Irrigat. Drain. Eng. 138 (11) (2012) 1011–1018.
[13] V. Ferro, New theoretical solution of the stage-discharge relationship for sharp-crested and broad weirs, Journal of Irrigation and Drainage Engineering, ASCE 138 (3) (2012) 257–265.
[14] V. Ferro, Closure to "New theoretical solution of the stage-discharge relationship for sharp-crested and broad weirs" by V. Ferro, Journal of Irrigation and Drainage Engineering, ASCE 139 (6) (2013) 518–520.
[15] M. Bijankhan, C. DiStefano, V. Ferro, S. Kouchakzadeh, New-stage discharge relationship for weirs of finite crest length, Journal of Irrigation and Drainage Engineering, ASCE 140 (3) (2014) 06013006-1 - 06013006-8.
[16] M. Bijankhan, C. DiStefano, V. Ferro, Generalised stage-discharge relationship for rectangular weirs, Water Management 1–9 (2017), https://doi.org/10.1680/wama.1600102.
[17] M. Bijankhan, V. Ferro, Dimensional analysis and stage-discharge relationship for weirs: a review, Journal of Agricultural Engineering XLVIII (2017) 1–11.
[18] M. Bijankhan, V. Ferro, Experimental study and numerical simulation of inclined rectangular weirs, J. Irrigat. Drain. Eng. 144 (7) (2018) ASCE.
[19] Z. Oreizi, M. Heidarpour, S. Bagheri, Hydraulic characteristics of flow over sinusoidal sharp-crested weirs, J. Irrigat. Drain. Eng. 141 (3) (2014) 06014003-1-5.
[20] W.H. Hager, Discharge Measurement Structure, Communication, Ecole Polytechnique, Lausanne, 1986 63 pp..
[21] S. Wu, N. Rajaratnam, Submerged flow regimes of rectangular sharp-crested weirs, J. Hydrol. Eng. 122 (7) (1996) 412–414.
[22] A.H. Azimi, N. Rajaratnam, D.Z. Zhu, Submerged flows over rectangular weirs of finite crest length, J. Irrigat. Drain. Eng. 140 (2) (2014) 148–160.
[23] A.H. Azimi, Y. Qian, D.Z. Zhu, N. Rajaratnam, An experimental study on circular slurry wall jets, Int. J. Multiph. Flow 74 (2015) 34–44.
[24] A.H. Azimi, N. Rajaratnam, D.Z. Zhu, Water surface characteristics for submerged rectangular sharp-crested weirs, J. Hydraul. Eng. 142 (5) (2016) 06016001-9.
[25] S. Hakim, A.H. Azimi, Submerged flows over triangular weirs and of finite crest length with upstream and downstream ramps, J. Irrigat. Drain. Eng. 143 (8) (2017) 06017008-1-12.
[26] R.H. French, Open Channel Hydraulics, McGraw-Hill, New York, NY, 1986.
[27] J.K. Vennard, R.F. Weston, Submergence effect on sharp crested weirs, Eng. News Rec. 130 (22) (1943) 814–816.
[28] J.R. Villemonte, Submerged weir discharge studies, Eng. News Rec. 866 (1947) 54–57.
[29] N. Rajaratnam, D. Muralidhar, Pressure and velocity distribution for sharp-crested weirs, J. Hydraul. Res. 9 (2) (1971) 241–248.
[30] M. Bijankhan, S. Kouchakzadeh, Unified discharge coefficient formula for free and submerged triangular labyrinth weirs, Flow Meas. Instrum. 57 (2017) 46–56.
[31] T.L. Wahl, Analyzing ADV Data Using WinADV, Proc., Joint Conf. On Water Resources Engineering and Water Resources Planning and Management, ASCE, Reston, VA, 2000 10pp..
[32] D.C. Wilcox, Turbulence Modeling for CFD, DCW Industries, La Canada, CA, 1993 522 pp..